2019 American Control Conference (ACC)
Philadelphia, PA, USA, July 10-12, 2019

MPC-trained ANFIS for Control of MicroCSP Integrated into a Building HVAC System

Mohamed Toub[1], Mahdi Shahbakhti[2], Rush D. Robinett III[2], and Ghassane Aniba[1]

Abstract— **This paper presents the design of an easily implementable rule-based controller that can minimize the electrical energy consumption of a building heating, ventilation, and air-conditioning (HVAC) system integrated with a micro-scale concentrated solar power (MicroCSP) system. A model predictive control (MPC) scheme is developed to optimize MicroCSP electrical and thermal energy flows for HVAC use in a building. Despite its attractiveness regarding energy savings and thermal comfort satisfaction, MPC requires high computational resources and can not be easily implemented on the common low-cost HVAC controllers available in the market. To cope with these issues, two MPC-trained adaptive neuro-fuzzy inference system (ANFIS) models are designed to control the building HVAC with MicroCSP. Simulation results exploiting real operation data from an office building at Michigan Technological University and our newly purchased MicroCSP are presented. It is shown that the resulting controller can reproduce the MPC reasoning and performance while being simpler and much more computationally efficient.**

I. INTRODUCTION

The energy-intensive nature of the heating, ventilation, and air-conditioning (HVAC) equipment in buildings and their associated CO_2 emissions, makes them an important parts of energy efficiency programs in the U.S. One of the key solutions to reduce the electrical energy consumption of the building HVAC systems is their hybridization with renewable solar energy resources. Indeed, solar-assisted HVAC systems are well studied in the literature. The authors in reference [1] built a solar-thermal-assisted HVAC system to produce and store heat in a thermal energy storage (TES) system so that it can be used to provide either heating or cooling to a university campus building. They were able to achieve a 30% annual cost saving using day-ahead scheduling. A hybrid solar-assisted HVAC and water heating system was presented in reference [2]. The authors used a rolling stochastic optimization approach for smart scheduling of the energy and showed a significant reduction of the energy cost. In another study in reference [3], several hybrid systems including photovoltaic (PV), micro-CHP (combined heat and power), and solar thermal were simulated to investigate their potential in reducing the emissions and energy consumption in a building.

*This work is supported in part by the US National Science Foundation (Grant #1541148), the Richard and Elizabeth Henes Professorship of Mechanical Engineering at Michigan Technological University, and the Institute for Research on Solar and New Energies (IRESEN) in Morocco (reference: InnoTherm-13-MicroCSP).

[1]Mohammadia School of Engineering, Mohammed V University of Rabat, Rabat, Morocco mohamedtoub@research.emi.ac.ma, ghassane@emi.ac.ma

[2]Michigan Technological University, Houghton, MI, USA {mahdish, rdrobine}@mtu.edu

The conventional On/Off rule-based controllers (RBC) are the most commonly used controllers for HVAC systems due to their simplicity and easy implementation. To ensure thermal comfort, the RBC checks the thermal zone air temperature at each time step. When the temperature is outside the comfort temperature bound, the RBC switches on the heating or cooling elements for the time step period Δt until it is again within the comfort temperature bound. The HVAC controllers usually include microprocessors with low computational power. These controllers are suitable for implementing RBC but require significant resources for implementing advanced model predictive controllers (MPC) [4].

The intermittent behavior of solar energy and its limitation to the daytime hinder the use of RBC for the control of solar energy integrated into building HVAC systems. Hence, more advanced control methods such as MPC can be used. MPC has been extensively studied in the literature for control of building HVAC systems with heat pumps (HP) [5], PV arrays with batteries [6], or MicroCSP with TES [7]. The authors in reference [8] presented a hierarchical MPC for a building energy management system. They developed a modular coordination method of MPC for microgrid energy flows and building zone comfort to minimize the operation cost of the building. In reference [9], the authors presented a hybrid MPC strategy to control solar-assisted HVAC. The air-based PV-thermal system, the phase change active storage, and the residential building HVAC system were optimally controlled to ensure thermal comfort efficiently.

Although MPC offers attractive features in terms of real-time optimization for minimal energy consumption and thermal comfort satisfaction, MPC for building HVAC control requires solving optimization problems that are usually complex, time-consuming, and memory intensive. To cope with these drawbacks, the authors in reference [10] proposed two MPC-inspired regressor-based feedback controllers for a building HVAC system. They were able to capture the MPC capabilities to minimize energy consumption while ensuring thermal comfort. Another possible approach to approximating MPC performance is adaptive neuro-fuzzy inference system (ANFIS). ANFIS was used in reference [11] for accurate prediction of the damping ratio of the HVAC system dampers. The authors showed that the predicted damping ratio, using ANFIS, achieved accurate tracking of the set values for temperature and relative humidity. In reference [12], the authors compared an ANFIS-based controller with other artificial intelligence control methods for building thermal control. They concluded that ANFIS-based controller, along with artificial neural network controllers, can guarantee

desired temperature set-points tracking to ensure thermal comfort.

This paper proposes an ANFIS model that can mimic the MPC to control the MicroCSP integrated into the building HVAC and minimize the energy consumption while meeting the thermal comfort requirements. To the best of the authors' knowledge, this is the first study undertaken to design an MPC-trained ANFIS controller for the optimal integration of solar energy into a building HVAC system. The results are presented for a real building test bed and actual MicroCSP system. The extracted rules from ANFIS can easily be implemented in an RBC.

II. Building Test Bed

The Michigan Technological University Lakeshore Center is the building test bed investigated in this work. It is an office building with three floors of 5,700 m^2 area each. An individual thermal zone in the test bed is a room or an office heated by an individual HP. Each thermal zone is equipped with a thermocouple recording the temperature data with $\pm 0.2\ ^{o}$C accuracy at a 1-minute sampling rate.

The supply air temperature is controlled to adjust the temperature of the thermal zones, while the mass flow rate of the supply air is kept constant and proportional to the thermal zone area. Fig. 1 shows the test bed setup in this study.

III. Modeling

A. Parabolic Trough Collectors (PTC)

In this paper, a three-row solar array is considered. The solar array is composed of PTC from Soltigua, model PTMx-24 [7]. Each row is equipped with a north-south axis tracking system allowing sun tracking from east to west.

The thermal power generated by the PTC in the solar array is the solar thermal power ($\dot{Q}_{abs}$) absorbed minus the heat losses ($\dot{Q}_{loss}$):

$$\dot{Q}_{SOL} = \overbrace{\eta_o.DNI.\cos(\theta).A_p.IAM}^{\dot{Q}_{abs}} - \overbrace{a_1.\frac{(T_{htf}-T_{amb})}{DNI}}^{\dot{Q}_{loss}} \quad (1)$$

where, η_o is the optical efficiency of the collectors; DNI is the direct normal irradiance; θ is the incidence angle calculated from reference [13]; A_p is the area of the aperture; IAM is the incident angle modifier interpolated as a second order correction function from table based values provided by the PTC manufacturer [7]; a_1 is the heat loss coefficient taken from the PTC manufacturer datasheet; and T_{amb} is the temperature of the outdoor ambient air. Since the temperature of the heat transfer fluid (HTF) is assumed to be increasing linearly through the collectors, T_{htf} is the average HTF temperature in the solar array.

B. Thermal Energy Storage (TES)

The TES system considered in this paper is a two-tank direct TES system as shown in Fig. 1. Each tank is modeled as a fully-mixed tank with a cylindrical shape that can contain the entire quantity of the HTF. In charging mode, the solar array absorbs the low-temperature HTF from the cold tank and charges the hot tank with the produced high-temperature HTF. In discharging mode, the hot tank discharges the high-temperature HTF in the ORC that converts the thermal energy contained in the HTF into electrical energy and cogenerated heat. Then reinjects the low-temperature HTF in the cold tank.

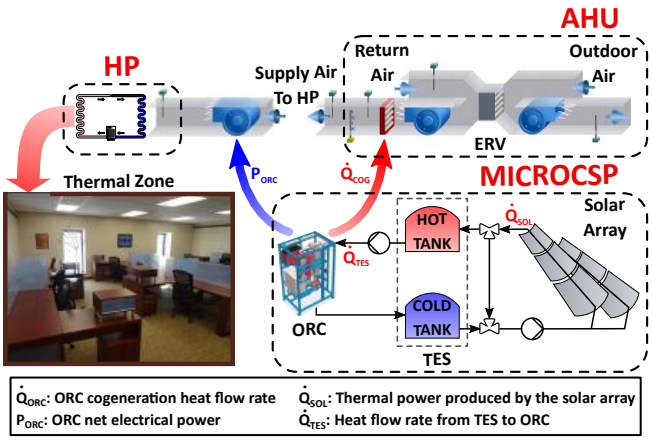

Fig. 1. MicroCSP and building HVAC setup in this study.

Assuming the tanks are well insulated, the heat losses in the tanks are neglected since the TES does not provide overnight storage. The TES system stores the energy from the solar array which will be used to run the ORC at its maximum efficiency when thermal and electrical energies are needed by the building during the day and till midnight. Hence, the TES mitigates the intermittency of the solar array generation to guarantee efficient and reliable power supply through the ORC.

To estimate the TES state of charge (SOC), the following equation is used

$$\dot{SOC} = \frac{\dot{Q}_{SOL} - \dot{Q}_{TES}}{C_{TES}} \quad (2)$$

where, $\dot{Q}_{TES}$ is the thermal power dispatched from the TES to the ORC; and C_{TES} is the thermal capacity of the TES.

C. Organic Rankine Cycle (ORC)

In this paper, a low-temperature ORC engine with a 10 kW nominal power manufactured by ENOGIA, model ENO-10LT [7] is considered with the Pentafluoropropane R245fa as a working fluid (WF).

By applying the First Law of Thermodynamics to the WF closed system, it can be shown that the ORC electrical power production (P_{ORC}) and cogenerated thermal power ($\dot{Q}_{ORC}$) are functions of the ORC turbine pressure ratio (r_p) and the mass flow rate of the HTF dispatched from the TES to the ORC ($\dot{m}_{tes}$):

$$\dot{Q}_{ORC} = f(\dot{m}_{tes}, r_p) \quad (3a)$$

$$P_{ORC} = g(\dot{m}_{tes}, r_p) \quad (3b)$$

where, f and g are fit functions from experimental data [7].

D. Building Thermal Model

The thermal model of the building test bed studied in this paper is derived by applying the well-known RC modeling technique that uses resistive, capacitive, and current

elements to model storage and heat transfer with outdoor and contiguous thermal zones. The building test bed model is detailed and experimentally validated in our previous works in references [5], [14], and [15].

To calculate the building HVAC energy consumption, the energy index ($I_{e,t}$) is determined by:

$$I_{e,t} = \sum_{t=0}^{t_f} \sum_{i=1}^{N_z} \left(P_{i,t}^{F} + P_{i,t}^{HP} \right) .\Delta t \tag{4}$$

where, Δt is the time step; and N_z is the number of thermal zones in the building considered for this study. The main focus of this study is the heating mode, hence the HVAC electrical consumption is the total of the electrical power consumed by the HP ($P_{i,t}^{HP}$) and by the ventilation fans ($P_{i,t}^{F}$):

$$P_{i,t}^{HP} = \frac{\dot{m}_{i,t}^{r} . c_{p,air} . (\mathcal{T}_{i,t}^{su} - T_{i,t}^{HP})}{COP} \tag{5a}$$

$$P_{i,t}^{F} = \gamma_F . (\dot{m}_{i,t}^{r})^3 \tag{5b}$$

where, $\dot{m}_i^r$ and $\mathcal{T}^{su}$ are the mass flow rate and the temperature of the supply air, respectively; $T_{i,t}^{HP}$ is the HP inlet air temperature; COP is the coefficient of performance of the HP; γ_F is the fan power coefficient.

During the non-occupancy period, the air returning from the thermal zones is recirculated through the ORC condenser before going to the HP. During the occupancy period, the ventilation requirement defined by the ANSI/ASHRAE Standard 62.1-2007 for required indoor air quality is considered to calculate the minimum required mass flow rate ($\dot{m}_i^v$) of fresh air from the energy recovery ventilator (ERV) that will be mixed with the returning air from the thermal zones. The resulting mixed air goes through the ORC condenser and is heated, using the cogeneration heat ($\dot{Q}_{COG}$), to supply hot air to the HP or to the thermal zones directly. The inlet air temperature of each individual HP is calculated using Eq. (6a) for occupancy period and Eq. (6b) for the non-occupancy period.

$$T_{i,t}^{HP} = \frac{\dot{m}_{i,t}^{r} - \dot{m}_{i,t}^{v}}{\dot{m}_{i,t}^{r}} . T_{i,t}^{r} + \frac{\dot{m}_{i,t}^{v}}{\dot{m}_{i,t}^{r}} . T_{t}^{ERV} + \frac{\dot{Q}_{COG,t}}{N_z . \dot{m}_{i,t}^{r} . c_{p,air}} \tag{6a}$$

$$T_{i,t}^{HP} = T_{i,t}^{r} + \frac{\dot{Q}_{COG,t}}{N_z . \dot{m}_{i,t}^{r} . c_{p,air}} \tag{6b}$$

The temperature of the ERV outlet (T^{ERV}) is:

$$T_{t}^{ERV} = T_{amb,t} + ERE . (T_{i,t}^{r} - T_{amb,t}) \tag{7}$$

where, ERE is the energy recovery effectiveness of the ERV defined by the AHRI (Air-Conditioning, Heating and Refrigeration Institute) Standard 1060 and the ASHRAE Standard 84.

IV. Building Model Predictive Control (MPC)

Here, an MPC framework is designed to minimize the electrical energy consumption of the building HVAC system equipped with the MicroCSP. At each time step Δt, the optimization problem is solved over the prediction horizon N. Eq. (8) defines the objective function subject to the constraints listed in Eq. (9). The optimized variables are the supply air temperature ($\mathcal{T}^{su}$) and the HTF mass flow rate from the TES ($\dot{m}_{tes}$). The inputs to the MPC optimizer are solar irradiation and weather forecasts. The comfort temperature bounds are set based on ANSI/ASHRAE Standard 55-2013.

$$\underset{\mathcal{T}^{su}, \dot{m}_{tes}, \underline{\epsilon}, \bar{\epsilon}}{\text{MIN}} \left((I_{e,t} - \sum_{t=0}^{t_f} P_{ORC,t} . \Delta t) + \rho . (|\underline{\epsilon}|_1 + |\bar{\epsilon}|_1) \right) \tag{8}$$

Subject to the constraints:

$$T_{t+k+1|t} = A . T_{t+k|t} + B . \mathcal{T}_{t+k|t}^{su} + E . d_{t+k|t} \tag{9a}$$

$$T_{t+k|t}^{r} = C . T_{t+k|t} \tag{9b}$$

$$\dot{Q}_{COG,t+k|t} = f(\dot{m}_{tes_{t+k|t}}) \tag{9c}$$

$$P_{ORC,t+k|t} = g(\dot{m}_{tes_{t+k|t}}) \tag{9d}$$

$$SOC_{t+k+1|t} = SOC_{t+k|t} + \frac{(\dot{Q}_{SOL_{t+k|t}} - \dot{Q}_{TES_{t+k|t}}) . \Delta t}{C_{TES}} \tag{9e}$$

$$\underline{SOC} \leq SOC_{t+k+1|t} \leq \overline{SOC} \tag{9f}$$

$$0 \leq \dot{m}_{tes_{t+k|t}} \leq \dot{m}_{max} \tag{9g}$$

$$T_{t+k|t}^{HP} \leq \mathcal{T}_{t+k|t}^{su} \leq \bar{T}_{t+k|t} \tag{9h}$$

$$\underline{T}_{t+k|t}^{r} - \underline{\epsilon}_{t+k|t} \leq T_{t+k|t}^{r} \leq \bar{T}_{t+k|t}^{r} + \bar{\epsilon}_{t+k|t} \tag{9i}$$

$$\underline{\epsilon}_{t+k|t}, \bar{\epsilon}_{t+k|t} \geq 0 \tag{9j}$$

The state-space model of the building thermodynamics is represented in Eq. (9a) and (9b); (9c) and (9d) include the ORC model; (9e) estimates the SOC of the TES; (9f) defines the upper and lower bounds of the SOC set to 5% and 95%, respectively; (9g) is the maximum HTF mass flow rate ($\dot{m}_{max}$) dictated by the ORC manufacturer; (9h) shows the constraints on the supply air temperature according to the HP settings; (9i) defines the comfort temperature bounds of the thermal zone air temperature; finally, (9j) includes temperature soft constraints that uses slack variables to ensure a feasible optimal solution at all times.

V. Adaptive Neuro-Fuzzy Inference System

ANFIS is a neuro-fuzzy-based hybrid model with a structure and learning ability similar to a neural network, and a behavior and reasoning comparable to a Sugeno-type FIS [16]. Fig. 2 shows the general structure of an ANFIS model composed of five layers:

1) Layer I: The nodes in this layer represent membership functions that map each input x_i to a membership value. Hence, the node function of the ith node is:

$$O_i^1 = \mu_{A_i}(x_i) \tag{10}$$

where, μ_{A_i} is the membership function associated with the linguistic label A_i; and x_i is the input to the node.

2) Layer II: Each node in this layer represents an if-then rule. The output of this layer is the firing strength of the rule. The ith node function is a T-norm operator that performs the generalized AND operator. Usually, the multiplication of the degrees of memberships of the input signals is used:

$$O_i^2 = w_i = \prod_i \mu_{A_i}(x_i) \tag{11}$$

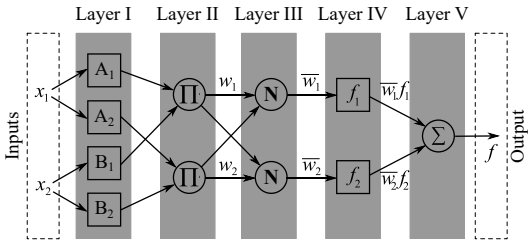

Fig. 2. ANFIS model general structure.

3) Layer III: Nodes in this layer are norm nodes that calculate the normalized firing strength which is the ratio of the firing strength of the ith rule to the sum of the firing strengths of all rules. Hence, the ith node function is:

$$O_i^3 = \overline{w}_i = \frac{w_i}{\sum w_j} \tag{12}$$

4) Layer IV: The node functions in this layer are:

$$O_i^4 = \overline{w}_i f_i = \overline{w}_i (p_i x + q_i y + \cdots + r_i) \tag{13}$$

5) Layer V: This node contains a single node that performs the summation of all inputs to produce the overall output of the ANFIS:

$$O_i^5 = \sum \overline{w}_i f_i \tag{14}$$

Two ANFIS models are designed and trained using data from the MPC results for broad building operating range.

The SOC of the TES and the temperature difference (ΔT) between the thermal zone air temperature and the lower comfort temperature bound are used as inputs for the first ANFIS model and the thermal power dispatched from the TES is used as the ANFIS model output. This ANFIS model has to decide on the amount of heat to be dispatched from the TES in order to minimize the energy consumption while keeping the thermal zone air temperature within the comfort temperature bounds. To make such a decision, the ANFIS model must know the SOC of the TES and how far is the thermal zone air temperature from the lower bound.

After the decision on the amount of heat dispatched from the TES is made, the second ANFIS model takes this information as input along with the difference between the thermal zone air temperature and the lower comfort temperature bound. Then, it decides how much heat is still needed from the HP to ensure that the thermal zone air temperature is inside the comfort temperature bounds and commands the required supply air temperature.

Fig. 3(a) presents the output surface for the first ANFIS model. It depicts the rules that the model has learned during the training process. As it can be seen, when the difference between the thermal zone air temperature and the lower comfort temperature bound is near zero, the ANFIS dispatches heat ($\dot{Q}_{TES}$) from the TES to maintain the thermal zone air temperature close to the lower comfort temperature bound avoiding unnecessary heating of the thermal zone. On the other hand, the ANFIS dispatches heat from the TES only when the SOC of the TES is high enough to supply thermal power to the ORC close to its optimal input (60 kW) that maximizes its efficiency.

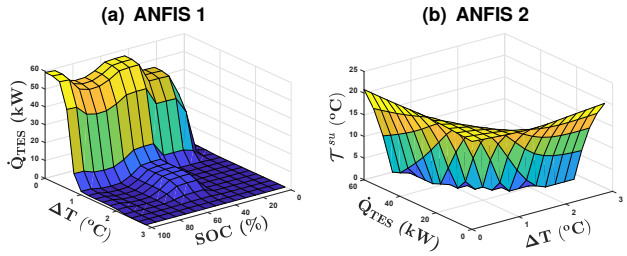

Fig. 3. ANFIS output surfaces.

The output surface for the second ANFIS model is shown in Fig. 3(b). It can be seen that the supply air temperature to the thermal zone decreases when the thermal zone air temperature is higher than the lower comfort temperature bound and/or the heat dispatched from the TES is high.

VI. Results

MATLAB® software was used to implement the building, solar array, TES, and ORC models. YALMIP Toolbox was used in MATLAB® for the optimization problem formulation and providing an interface with the Gurobi solver. For the adaptive neuro-fuzzy modeling, the Fuzzy Logic Toolbox™ was used. The simulations were done in a computer with a processor Intel® Core™ i7-7500 CPU @ 2.90GHz and 16.0 GB RAM.

The prediction horizon is N = 48, and the time step is Δt = 30 minutes. 72 thermal zones are considered for the building simulation. The simulations are performed using weather data from March 18, 2016, in Houghton, MI. It is important to mention that *this data is different from the data used for ANFIS training* which was generated manually to simulate different scenarios for irradiation and outdoor ambient temperature.

A. MPC Results

The MPC results of the combined building HVAC and MicroCSP are shown in Fig. 4. Fig. 4(a) depicts the temperature profiles of the supply air and a sample thermal zone within the comfort temperature bounds. It can be seen that before 6 AM during the non-occupancy period, the HP is turned off and the thermal zone temperature decreases within the comfort temperature bounds. After 6 AM during the building occupancy period, the thermal zone is supplied with the minimum amount of heat to maintain its temperature at the lower comfort temperature bound, hence minimizing the HVAC energy consumption. Fig. 4(b) shows the thermal power generated by the solar array and the thermal power dispatched from the TES to the ORC. From Fig. 4(c), it can be seen that the main source of heat for the building is the MicroCSP cogeneration whereas the HP supplies the required heat only when there is not enough heat in the TES to run the ORC. The power supplied from the electric grid and from the ORC to the building are shown in Fig. 4(d). The TES stores the extra heat generated by the solar array that is not used by the ORC so that it can be recovered when needed. The variation of the SOC of the TES is shown in Fig. 4(e) and confirms that all the solar energy is used; thus, the initial and final SOCs are the same.

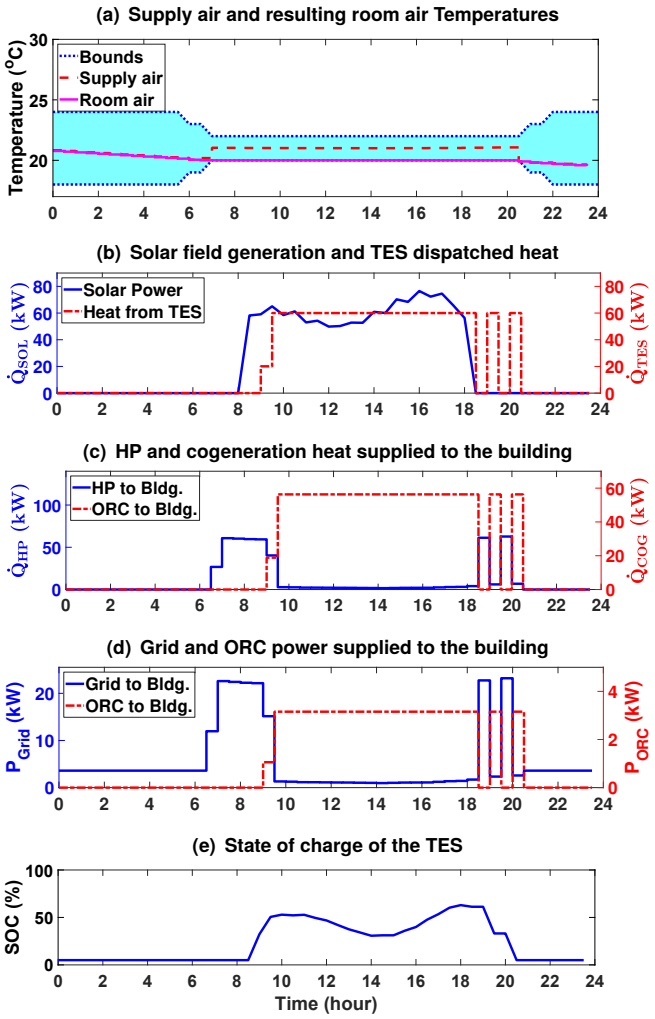

Fig. 4. MPC control results for the combined HVAC and MicroCSP.

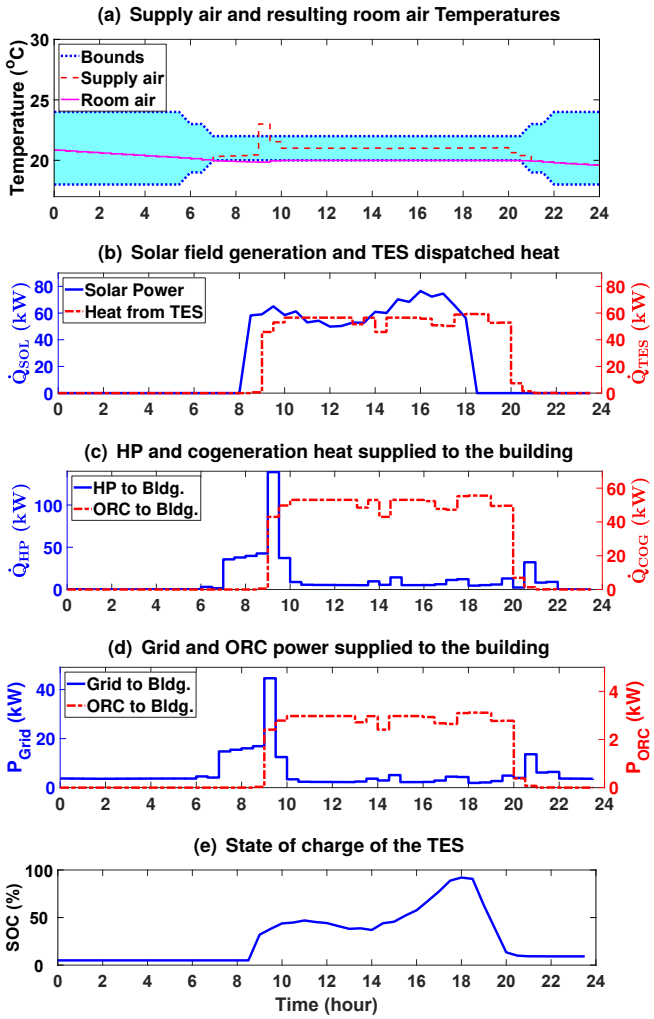

Fig. 5. ANFIS control results for the combined HVAC and MicroCSP.

B. MPC-Inspired ANFIS Controller Results

Fig. 5 shows the ANFIS control results for energy minimization of the building HVAC with MicroCSP. As shown in Fig. 5(a), the ANFIS controller mimics the MPC by keeping the thermal zone air temperature on the lower bound to minimize energy consumption and avoid unnecessary overheating. Note that, at the beginning of the occupancy period, a temperature violation can be observed. This is due to the fact that the ANFIS controller doesn't have the predictive capability of the MPC and cannot anticipate this temperature violation. Regarding the dispatched thermal power from the TES to the ORC, the ANFIS controller tries to maximize the efficiency by keeping the TES output as close as possible to the nominal input of the ORC as shown in Fig. 5(b). The trained ANFIS controller is able to avoid the violation of the SOC constraints (Fig. 5(e)).

The energy saving and the computational cost of the original MPC and the MPC-trained ANFIS compared to the conventional RBC are summarized in Table I. It can be seen that the building HVAC energy saving using MPC is just 4% higher compared to using the ANFIS controller. But, the MPC controller requires ten times more computation time to generate the optimal solution, compared to the trained ANFIS controller. This result is of high importance if one considers that the HVAC controllers in the marketplace are mostly based on microprocessors with limited computational capability.

C. Probabilistic Monte-Carlo Analysis

The ANFIS controller results can be subject to interpretation since they are valid only for the chosen simulation day conditions and will change with variations in solar irradiation and weather conditions. Hence, to demonstrate the validity of the ANFIS controller performance, a Monte-Carlo analysis is carried out by introducing additive uncertainty with a normal distribution to simulate random variations of weather condition and solar irradiation, using results from [6]. Fig. 6(a) shows the probability distribution of the energy saving of the building HVAC integrating MicroCSP with the

TABLE I

COMPARISON TABLE FOR THREE DIFFERENT HVAC CONTROLLERS

Control Type	Elec. Consumption [kWh/day]	Energy Saving* [%]	Computational Cost [s]
RBC	193.2	-	5.4
MPC	130.3	32.7%	117.6
ANFIS	138.5	28.3%	11.9

*Calculated by comparison with RBC of building HVAC system with MicroCSP.

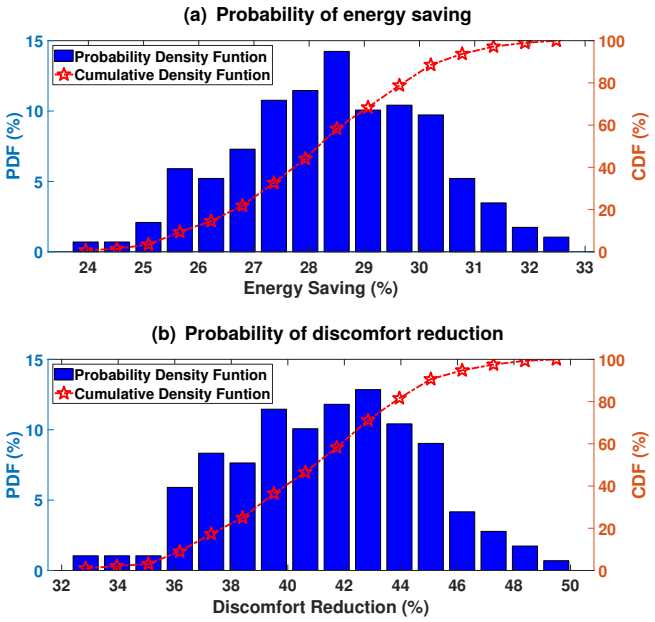

Fig. 6. Monte-Carlo analysis results

ANFIS controller compared to the RBC. It can be seen that there is a 70% probability for providing up to 29% energy saving. Furthermore, it can be seen that the energy saving drops to 24% in the worst case scenario.

The results shown in Fig. 6 confirm that the ANFIS controller can still save energy even in the case of variable solar irradiation and weather conditions. However, energy saving is not the only important feature of building climate control systems, the thermal comfort of users is also an important metric. Thus, a discomfort index is calculated in this study to capture the thermal comfort violation. As defined in [5], the discomfort index (I_d) sums up all the temperature violations during the day:

$$I_d = \sum_{t=0}^{t_f} min(|T_t^r - \underline{T}_t^r|, |T_t^r - \bar{T}_t^r|).\mathbf{1}_{\mathcal{B}^c(t)}(T_t^r) \qquad (15)$$

where, $\mathcal{B}(t) = [\underline{T}_t^r, \bar{T}_t^r]$ is the comfort zone set at time t, and $\mathbf{1}_{\mathcal{B}^c(t)}$ is the indicator function of its complement $\mathcal{B}^c(t)$.

Fig. 6(b). shows that the discomfort index of the ANFIS controller is 40% lower than the RBC in 50% of the cases. The ANFIS controller reduces the discomfort index by at least 32% compared to the RBC. The I_d for ANFIS results ranges from 0.27 to 0.36 ^{o}Ch. This shows that the ANFIS controller is able to maintain desired indoor thermal comfort conditions with minimal violations even with the presence of variations in the weather conditions and the solar irradiation.

VII. CONCLUSIONS

This paper presents the first MPC-inspired ANFIS framework for the control of MicroCSP integrated with a building HVAC system. The simulation results show that the performance of the proposed ANFIS framework is close to the MPC with regard to energy consumption savings and thermal comfort satisfaction. The ANFIS controller provided 28% energy saving compared to the RBC, while MPC energy saving was 32% (approximately 4% difference). However, the ANFIS rules have a simple structure that can be easily implemented on rule-based HVAC controllers. In addition, the computational time of the ANFIS controller is one order of magnitude less than the MPC.

Furthermore, a probabilistic analysis using Monte-Carlo simulations showed that the proposed ANFIS framework can guarantee suitable control performance (24% - 32% energy saving) even with variable weather conditions and solar irradiation. Combined with its low computational demand and its easy implementation, these features make the MPC-trained ANFIS controller a viable alternative to both complex MPC and basic RBC for the control of solar-assisted building HVAC systems.

REFERENCES

[1] A. Mammoli, P. Vorobieff, H. Barsun, R. Burnett, and D. Fisher. Energetic, economic and environmental performance of a solar-thermal-assisted HVAC system. *Energ. Buildings*, 42(9):1524–1535, 2010.

[2] H. T. Nguyen, D. T. Nguyen, and L. B. Le. Energy management for households with solar assisted thermal load considering renewable energy and price uncertainty. *IEEE Trans. on Smart Grid*, 6(1):301–314, 2015.

[3] L. R. Rodríguez, J. M. S. Lissén, J. S. Ramos, E. A. R. Jara, and S. A. Domínguez. Analysis of the economic feasibility and reduction of a building's energy consumption and emissions when integrating hybrid solar thermal/PV/micro-CHP systems. *Appl. Energy*, 165:828–838, 2016.

[4] G. Cimini and A. Bemporad. Exact Complexity Certification of Active-Set Methods for Quadratic Programming. *IEEE Trans. on Autom. Control.*, 62:6094–6109, 2017.

[5] M. Maasoumy, M. Razmara, M. Shahbakhti, and A. Sangiovanni Vincentelli. Handling model uncertainty in model predictive control for energy efficient buildings. *Energ. Buildings*, 77:377–392, 2014.

[6] M. Razmara, G. R. Bharati, D. Hanover, M. Shahbakhti, S. Paudyal, and R. D. Robinett III. Building-to-grid predictive power flow control for demand response and demand flexibility programs. *Appl. Energy*, 203:128–141, 2017.

[7] M. Toub, C. R. Reddy, M. Razmara, M. Shahbakhti, R. D. Robinett, and G. Aniba. Model Predictive Control for MicroCSP Integration into a Building HVAC System. In *The 14th IEEE Int. Conf. on Control and Automation*, pages 890–895, 2018.

[8] V. Lešić and M. Martinčević, A.and Vašak. Modular energy cost optimization for buildings with integrated microgrid. *Appl. Energy*, 197:14–28, 2017.

[9] M. Fiorentini, J. Wall, Z. Ma, J. H. Braslavsky, and P. Cooper. Hybrid model predictive control of a residential HVAC system with on-site thermal energy generation and storage. *Appl. Energy*, 187:465–479, 2017.

[10] E. Žáčeková, M. Pčolka, J. Tabačk, J. Těžký, R. Robinett, S. Čelikovský, and M. Šebek. Identification and energy efficient control for a building: Getting inspired by MPC. In *2015 American Control Conf. (ACC)*, pages 1671–1676, 2015.

[11] S. Soyguder and H. Alli. An expert system for the humidity and temperature control in HVAC systems using ANFIS and optimization with Fuzzy Modeling Approach. *Energ. Buildings*, 41(8):814–822, 2009.

[12] J. W. Moon, S. K. Jung, Y. Kim, and S. H. Han. Comparative study of artificial intelligence-based building thermal control methods – Application of fuzzy, adaptive neuro-fuzzy inference system, and artificial neural network. *Appl. Therm. Eng.*, 31(14-15):2422–2429, 2011.

[13] J. A. Duffie and W. A. Beckman. *Solar engineering of thermal processes*, chapter Solar Radiation. John Wiley & Sons, 2013.

[14] M. Maasoumy, M. Razmara, M. Shahbakhti, and A. Sangiovanni-Vincentelli. Selecting Building Predictive Control Based on Model Uncertainty. In *American Control Conf. (ACC)*, 2014.

[15] M. Razmara, G. R. Bharati, M. Shahbakhti, S. Paudyal, and R. D. Robinett. Bilevel optimization framework for smart building-to-grid systems. *IEEE Trans. on Smart Grid*, 9(2):582–593, 2018.

[16] M. Negnevitsky. *Artificial Intelligence: A Guide to Intelligent Systems*. Pearson Education Limited, 2011.